Vol. 26 • No. 48 • December 23 • 2014

www.advmat.de

ADVANCED MATERIALS

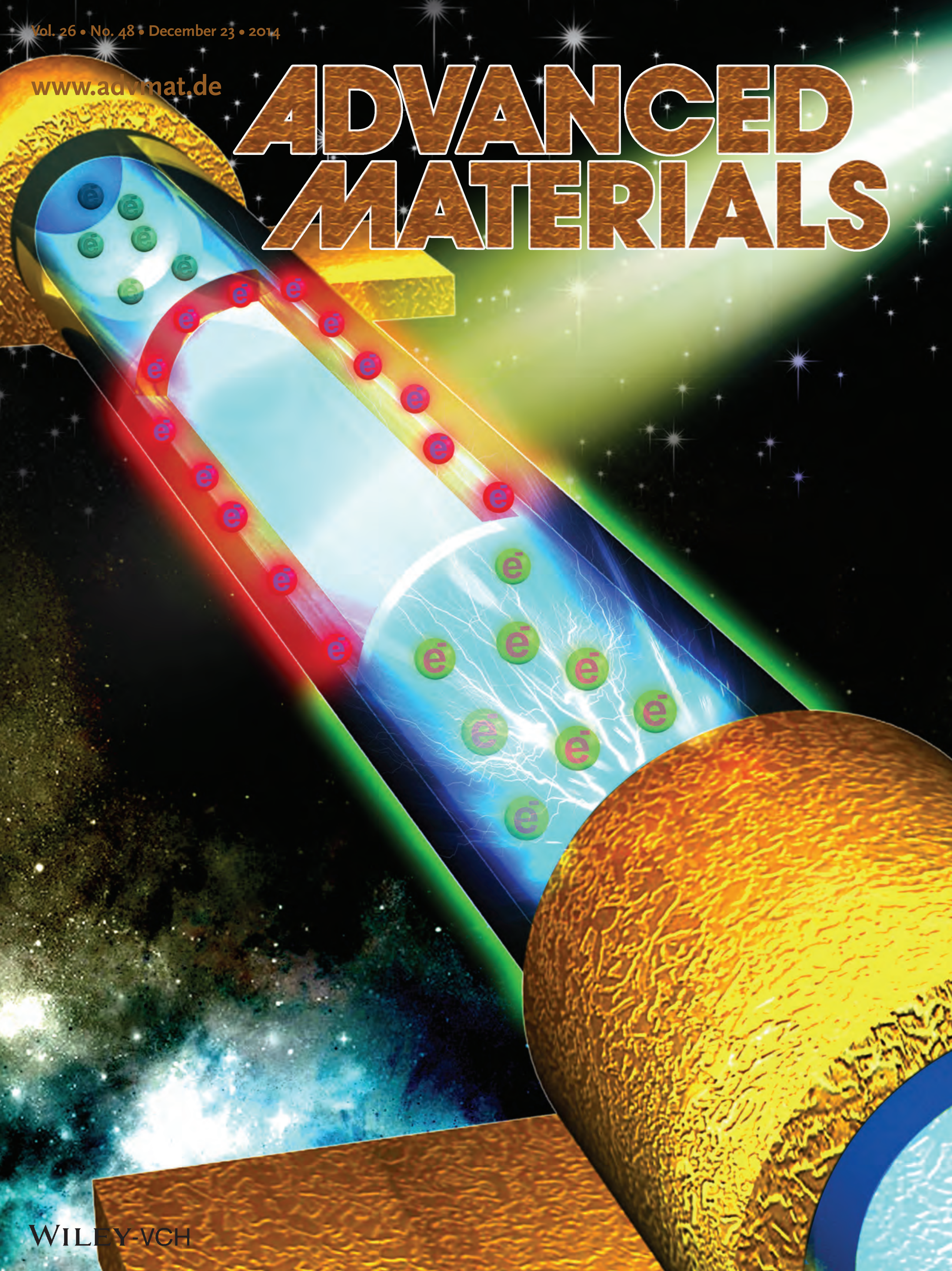

WILEY-VCH

Anomalous and Highly Efficient InAs Nanowire Phototransistors Based on Majority Carrier Transport at Room Temperature

Nan Guo, Weida Hu, Lei Liao,* SenPo Yip, Johnny C. Ho, Jinshui Miao, Zhi Zhang, Jin Zou, Tao Jiang, Shiwei Wu, Xiaoshuang Chen, and Wei Lu**

As important building blocks, semiconductor nanowires (NWs) have been paid extraordinary attention for their potential applications in nanoelectronics and nanophotonics in the recent decade.[1–22] As a result, many kinds of NWs have been grown and fabricated into devices to understand their photoconductive characteristics. Due to the large surface-to-volume ratio, the presence of surface states is expected to play an important role in photosensitivity,[21,23] and shorter effective conductive channels may bring on a faster transport speed.[23] InAs NWs, with a narrow bandgap of ca. 0.354 eV [24] and high carrier mobility at room temperature,[12] is an attractive material for applications in broad-spectrum detection, ranging from visible to infrared regions. However, there is a common problem for nearly all NW-based photodetectors: the short minority carrier lifetime. Quite a number of minority carriers are recombined before being collected by the contact to contribute the photocurrents. Soci et al.[21] reported that visible-blind UV photodetectors made of ZnO NWs have an internal photoconductive gain on the order of 10^8. Oxygen-related hole-trap states at the NW surface prolong the hole lifetime, leading to the extremely high photoconductive gain. Despite the excellent device performance, the photoresponse is completely suppressed in an oxygen-free environment and UV-light absorption also restricts the spectral range of photodetection. In addition, for most NW-based photodetectors reported so far, the photocurrent is mainly from the junction area, such as the NW–metal junction[16,25–29], the p–n junction[30–32] and the heterojunction. [33–36] Due to the small effective junction region and weak optical absorption, it is difficult to improve the device performance further, not to mention a complicated process for synthesis and device fabrication. Therefore, the minority-carrier transport mechanism and the junction-type device structure may become the bottleneck in pursuing the development of high-sensitivity broad-spectrum NW-based detectors in the future.

In this work, we design core/shell-like n-type InAs NWs grown by chemical vapor deposition (CVD), in which a self-assembled "photogating layer" (PGL) is formed near the NW surface by controlling the NW growth. The key function of the PGL, under light illumination, is of trapping electrons generated from the core. In return, the electrons maintaining trapped in the PGL form a built-in electric field to modulate the core conductance, i.e. a photogating effect.[37,38] In our design, the majority carriers, i.e., electrons, contribute to the photocurrent; thus, the whole channel of the NW, as the effective photosensitive region, responds to the light signal. A high photoconductive gain of ca. -10^5 and a fast response time of 12 ms are obtained at room temperature. In addition, compared with other NW-based detectors in which the response is largely restricted by gas molecules, our device shows excellent performance in both air and under vacuum. Utilizing the mechanism of majority-carrier-dominated photodetection enables high-sensitive broad-spectrum detection in NW-based transistors.

Figure 1a shows an illustration of the global back-gated core/shell-like InAs NW transistor configuration. The working principle can be understood through the schematic shown in Figure 1b,c. Before light illumination, the free electrons in the NW core flow under the action of the electric field to form the dark current, $I_{ds} > 0$ (see Figure 1b). Upon light exposure, the photogenerated electrons from the core are excited into the PGL (see Figure 1b) in which there are many randomly distributed trapping centers, leaving unpaired holes to recombine with the free electrons, which contributes to the dark current in the core immediately (see Figure 1c). Meanwhile, the maintaining trapped electrons in the PGL generate a built-in electric field to deplete free electrons in the core further through capacitive coupling (see Figure 1c). The synergistic effect of these two

Dr. N. Guo, Prof. W. D. Hu, J. S. Miao,
Prof. X. S. Chen, Prof. W. Lu
National Laboratory for Infrared Physics,
Shanghai Institute of Technical Physics
Chinese Academy of Sciences
500 Yutian Road, Shanghai 200083, China
E-mail: wdhu@mail.sitp.ac.cn
E-mail: luwei@mail.sitp.ac.cn
Prof. L. Liao
Department of Physics and Key Laboratory of Artificial
Micro- and Nano-structures of Ministry of Education
Wuhan University
Wuhan 430072, China
E-mail: liaolei@whu.edu.cn
Dr. S. P. Yip, Prof. J. C. Ho
Department of Physics and Materials Science
City University of Hong Kong
Hong Kong SAR, China
Dr. Z. Zhang, Prof. J. Zou
Material Engineering, The University of Queensland
St Lucia QLD 4072, Australia
Prof. J. Zou
Centre for Microscopy and Microanalysis
The University of Queensland
St Lucia QLD 4072, Australia
T. Jiang, Prof. S. W. Wu
State Key Laboratory of Surface Physics and Department of Physics
Fudan University
Shanghai 200433, China

DOI: 10.1002/adma.201403664

© 2014 WILEY-VCH Verlag GmbH & Co. KGaA, Weinheim

COMMUNICATION

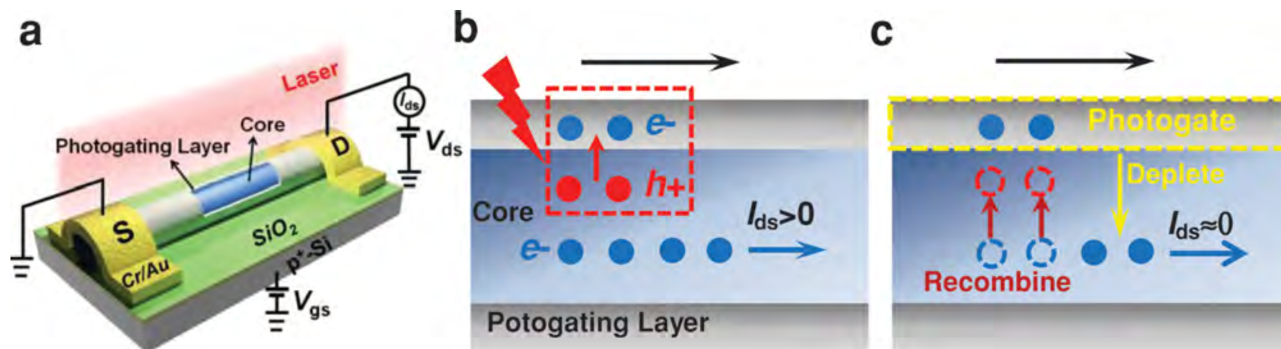

Figure 1. Schemetic for InAs NW phototransistor working principle. a) A schematic illustration of the InAs NW transistor. b) The process of photogenerated electron-hole pairs. Under light illumination, electrons (*e*-) are excited into the PGL and keep trapped. Holes (*h*+) are left in the NW core. c) The process of majority carrier dominated photodetection. Holes recombine with free electrons in the core. Electrons trapped in the PGL induce a photogating effect on the core.

factors results in a huge decrease in the photocurrent, $I_{ds} \approx 0$. In fact, the core/shell-like NWs have an identical composition to InAs, but the shell, i.e., the PGL, contains many randomly distributed lattice defects as trapping centers to capture photo-excited electrons.

In this work, InAs NWs were grown using a conventional CVD method.[39,40] By controlling the source temperature and the pressure in the growth chamber, we enabled the growth of core/shell-like NWs with perfect single crystal cores and highly defected shells. **Figure 2**a shows transmission electron microscopy (TEM) images of a typical NW. As can be observed in the low-magnification TEM image (refer to the inset in Figure 2a), the NW contains an uneven surface. The high-resolution TEM image shows that the NW has a well-crystallized core with a defected shell near the surface, referred to as the PGL. Figure 2b gives a scanning electron microscopy (SEM) image of a typical InAs NW transistor. The InAs NW as the channel material has a length of ca. 3.5 µm and a diameter of ca. 40 nm. The source/drain (S/D) electrodes (15 nm Cr and 60 nm Au) were prepared by electron-beam lithography, metallization, and the lift-off process. Figure 2c presents the I_{ds}–V_{ds} (ds refers to drain–source) characteristics of an as-fabricated InAs NW transistor measured both in the dark and under illumination from a green laser (532 nm, 8 mW mm^{-2}) in air. The I_{ds}–V_{ds} curve measured in the dark shows conventional long-channel transistor characteristics, i.e., a linear regime at low V_{ds} and a saturation regime at high V_{ds}.[41] The fact that the I_{Dark} (corresponding to the original current before the device was illuminated) increases with increasing V_{gs} (back-gate voltage) proves that the NW has an n-type characteristic. Upon light exposure, I_{Light} decreases dramatically to a very low level, in which a net photocurrent, defined as $I_{PC} = |I_{Light}| - |I_{Dark}$, as high as −4.5 µA is obtained at $V_{gs} = 40$ V and $V_{ds} = 1$ V (see Figure 2d). For a typical photodetector with a positive photoresponse, the photoconductive gain (G), defined as the number of charges collected by the electrodes due to the excitation by one photon, can be expressed as[20] $G = (I_{PC}/P)(h\nu/e)$, where $h\nu$ is the energy of an incident photon, e is the electron charge, and P is the light power absorbed by the NW channel. However, for the anomalous photoresponse based on the majority-carrier transport in this work, the negative photoconductive gain is defined as the number of carriers that "cannot be collected" by electrodes per incident photon. In order to

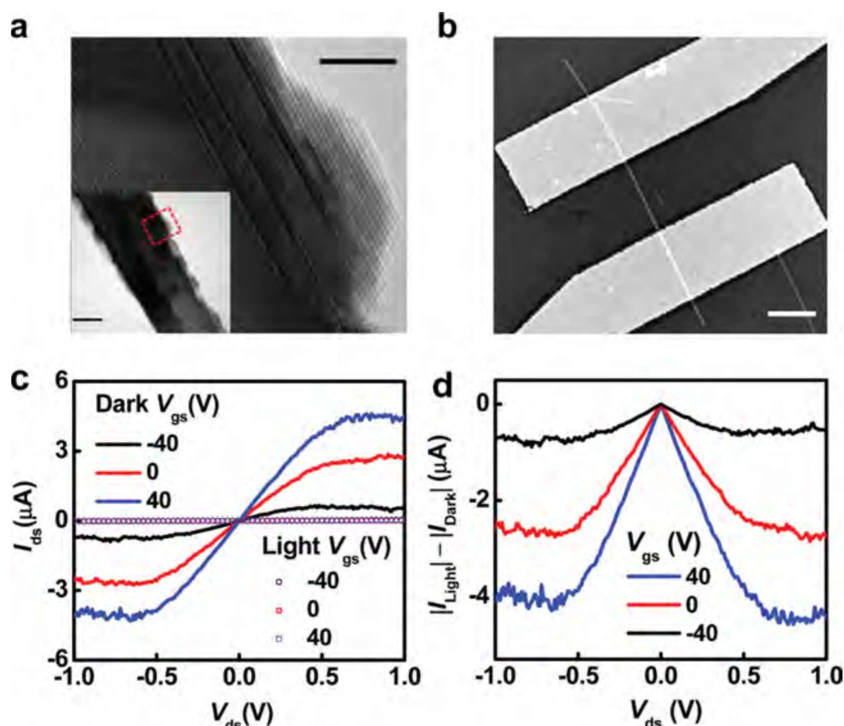

Figure 2. Core/shell-like InAs NW phototransistor. a) Bright-field TEM images of the InAs NW. The high-resolution TEM image (scale bar, 5 nm) is taken from marked region in the inset (scale bar, 20 nm). b) SEM image of the as-fabricated InAs NW transistor. Scale bar, 2 µm. c) I_{ds}–V_{ds} curves of the InAs NW transistor in the dark and under illumination from a green laser in air, recorded for different gate voltages. The wavelength is 532 nm and light intensity is 8 mW mm^{-2}. d) The net photocurrent, defined as $|I_{Light}| - |I_{Dark}|$, vs V_{ds}.

© 2014 WILEY-VCH Verlag GmbH & Co. KGaA, Weinheim

compare better with other NW detectors, which have a conventional positive photoresponse, we chose to adopt this similar definition. The only difference is that the gain is negative in this case. Under the assumption that light incident on the channel is absorbed completely, an ultrahigh negative gain of ca. -10^5 is obtained at $V_{gs} = 40$ V and $V_{ds} = 1$ V. As expected in our designed experiments, this extraordinary phenomenon originates from the majority-carrier-dominated photodetection mechanism as mentioned above. Figure S1 in the Supporting Information shows the I_{ds}–V_{ds} characteristics measured under illumination by a blue laser (445 nm, 8 mW mm^{-2}). The huge decrease of the photocurrent is comparable with that in Figure 2c.

To understand how the strength of the photogate changed with V_{gs} modulation, the photoresponse properties of InAs NW transistors under different back-gate voltages at V_{ds} = 1 V in air were investigated. The photoconductance modulation is realized by switching the incident light on and off alternately with an interval of 5 s. As shown in **Figure 3**a, the light modulation results in a "low" current state under illuminated conditions, (I_{on}), and a "high" current state under dark conditions, (I_{off}). The anomalous switching between these two states exhibits highly stable and reproducible characteristics. It is of interest to note that, in Figure 3a, $I_{Dark} \approx 3.7$ μA is found at V_{gs} = 40 V before illumination, but after the first 5 s of light exposure, $I_{off\text{-}step1}$ decreases to 2.5 μA, and after the second 5 s light exposure, $I_{off\text{-}step2}$ decreases to 2.25 μA. After that, I_{off} remains relatively stable ($I_{off}/I_{on} \approx 23$) under the light on/off cycles with a small fluctuation. Figure S2a in the Supporting Information shows the response following the light on/off cycles with V_{gs} = 0 V, in which $I_{off} \approx I_{Dark}$ and $I_{off}/I_{on} \approx 133$ can be obtained. When V_{gs} = −40 V, an opposite change appeared (refer to Figure S2b in the Supporting Information) when compared with the case shown in Figure 3a. The negative gate voltage leads to a reduced free electron density in the channel and in turn results in $I_{Dark} \approx 0.3$ μA. After the first 5 s of light exposure, $I_{off\text{-}step1}$ increases to 1.8 μA, and after the second 5 s of light exposure, $I_{off\text{-}step2}$ increases to 2.3 μA. After that, I_{off} remains at a stable high level following the light on/off cycles, in comparison with I_{Dark}, and I_{off}/I_{on} is found to be as high as 115. These phenomena will be explained later in detail.

In order to elucidate the effect of surface states on the anomalous photoresponse, the device responses, under vacuum and with a 10 nm HfO_2 passivation layer, have been studied, as shown in Figure S3 in the Supporting Information. The results illustrate that the device works well in both air and under vacuum. Also, importantly, the device performances are quite stable with/without the passivation layer. Recently, our group reported single-crystalline InAs NW photodetectors grown by molecular beam epitaxy, which had a positive photoresponse, in which the gas molecules and the passivation layer had a great impact on the photocurrent.[22] The chemical molecules adsorbed on the surface of the InAs NW not only change the band alignment to weaken the strength of built-in electric field of the NW–metal junction through electrostatic interactions, but also transfer photocarriers through the rich surface defect states to reduce the photocurrent. In that work, the HfO_2 passivation layer protected the NW from the ambient environment as well as surface defect states, to improve the device performance. However, the vacuum testing condition and passivation layer cannot affect the anomalous photoresponse in this work. Therefore, the effect of surface states is negligible in comparison with that of the photogating layer.

The response speed is a key parameter that determines the capability of a photodetector to follow a fast-varying optical signal.[20] Figure 3b shows a single normalized modulation cycle measured with a light intensity of 8 mW mm^{-2} at V_{gs} = 0 V and V_{ds} = 1 V. An oscilloscope was used to monitor the time dependence of the current.[20,23] The response time (falling time t_f), defined as the time necessary for the current to decrease from 90% I_{peak} to 10% I_{peak}, was found to be 12 ms in this case, and the recovery time (rising time t_r), defined analogously, was found to be 3.92 s. Furthermore, by respectively fitting the rising and falling edges with the equations $I = I_0[1 - A\exp(-t/\tau_{rec1}) - B\exp(-t/\tau_{rec2})]$ and

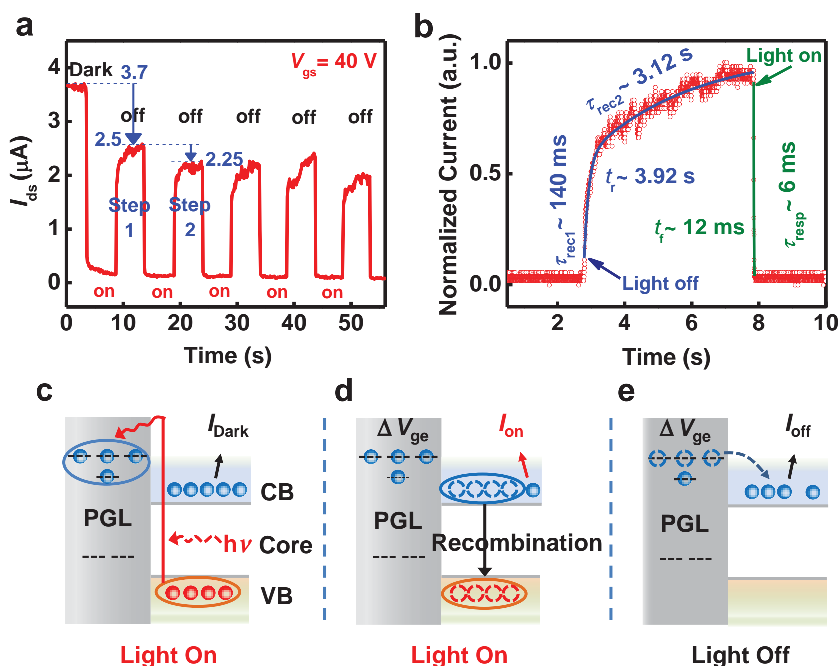

Figure 3. Photoresponse measurement of InAs NW phototransistor. a) Photoresponse properties of the InAs NW transistor under green laser illumination (532 nm, 8 mW mm^{-2}) at V_{ds} = 1 V in air, acquired for gate voltage of 40 V. The photoconductance modulation is induced by manipulating a shutter for the light on/off at an interval of 5 s. b) A single normalized modulation cycle measured with light intensity 8 mW mm^{-2} (open circles) at V_{gs} = 0 V and V_{ds} = 1 V. The blue and green lines fit to the rising (recovery τ_{rec1} and τ_{rec2}) and falling (response τ_{resp}) edges, respectively. c–e) Schematic of the energy-band diagrams of the InAs NW to illustrate the photoresponse mechanism. CB and VB are the conduction and valence band, respectively. ΔV_{ge} represents the negative photogate. The blue and red spheres represent electrons and holes, respectively.

© 2014 WILEY-VCH Verlag GmbH & Co. KGaA, Weinheim

$I = I_0[1 + C\exp(-t/\tau_{resp})]$, we can obtain two time constants τ_{rec1} (140 ms) and τ_{rec2} (3.12 s), which correspond to the fast and slow recovery processes, respectively, and can obtain one time constant τ_{resp} (6 ms) for the fast response process. τ_{rec1} and τ_{rec2} in the recovery process indicate the release process of the trapped photoexcited electrons from the PGL and the decay of photogating effect after the light was blocked, and τ_{resp} indicates the fast recombination process and the enhancement of photogating effect with light excitation. Figure S4 in the Supporting Information gives the response with different time intervals for the photoconductance modulation. It is obvious that the currents of the device (another sample in our work) can reach saturation point after 5 s when the light was blocked.

Based on the experimental observation outlined above, Figure 3c–e and Figure S5 in the Supporting Information schematically illustrate the photoresponse mechanism of NWs with PGLs. i) Upon light exposure with a photon energy larger than the NW bandgap, photogenerated electrons are excited into the PGL (see Figure 3c). Due to the positive V_{gs} of 40 V enhancing the electron density in the NW, corresponding to the situation shown in Figure 3a, all the photoexcited holes immediately recombine with most of the free electrons in the core that contribute to the conductivity in dark conditions. Simultaneously, the maintaining trapped electrons in the PGL produce a strong local negative photogate (ΔV_{ge}), leading to a further depletion of free electrons in the core through capacitive coupling (see Figure 3d). The recombination and depletion processes result in the rapid decrease of photocurrent, corresponding to the fast response process shown in Figure 3b (green line). In fact, Figure 3d illustrates an equilibrium physical process. With light illumination, the trapped electrons can also be released to the core, and then recombine and are depleted again. I_{on} is the result of the recombination–depletion–release cycle. When the light was blocked, the trapped electrons were released immediately from the PGL with decreasing ΔV_{ge} (see Figure 3e), i.e., the recovery process shown in Figure 3b (blue line), to contribute I_{off}. For the electrons trapped for a much longer time, they can still act as a small local negative photogate ΔV_{ge} on the n-type NW (see Figure 3e), a weak depletion in the core channel remains, and I_{off} weakens. Therefore, after the first 5 s light exposure, the existence of ΔV_{ge} results in a smaller $I_{off\text{-}step1}$ (2.5 μA) when compared with I_{Dark} (3.7 μA). However, 5 s of illumination is not sufficient to achieve equilibrium in this case. The current $I_{off\text{-}step2}$ (2.25 μA) continues to decrease following the footprint of $I_{off\text{-}step1}$ until the current reaches a stable state. ii) As V_{gs} decreases from 40 V to 0 V (refer to the situation in Figure S2a in the Supporting Information), the number of electrons in the channel is reduced (see Figure S5a in the Supporting Information). After all the free electrons in the core are recombined and depleted ($I_{on} \approx 0$), the remaining holes are also trapped by the PGL (see Figure S5b in the Supporting Information). With the light turned off, most of the trapped electrons in the PGL are released. At the same time, the holes that are trapped for a long time, also acting as a local positive photogate (ΔV_{gh}), can almost offset the effect of ΔV_{ge} (see Figure S5c in the Supporting Information). Hence, I_{off} is approximately equal to I_{Dark}. iii) For the situation shown in Figure S2b in the Supporting Information, $V_{gs} = -40$ V further lowered the free electrons density in the channel (see Figure S5d in the Supporting Information). Therefore, only a small fraction of photogenerated holes is needed to participate in the recombination process and the rest are trapped by the PGL (see Figure S5e in the Supporting Information). After the light was blocked, the photogenerated electrons that accumulated in the PGL during the first 5 s of light exposure are released to the core, resulting in an increasing $I_{off\text{-}step1}$. Simultaneously, since ΔV_{gh} induced by the accumulated holes in the PGL is much greater than ΔV_{ge} (see Figure S5f in the Supporting Information), the strong positive ΔV_{gh} significantly enhances the electron density in the core. Similarly, 5 s of illumination is not sufficient for equilibrium to be reached, so that the physical process will go on until I_{off} is stable. Hence, $I_{off\text{-}step2}$ (2.3 μA) continues to increase following the footprint of $I_{off\text{-}step1}$ (1.8 μA) until the current reaches a stable state. It is of interest to note that it is difficult for the photogenerated electrons and holes that are trapped for a long time to be released or recombined, as shown in Figure 3e and Figure S5c,f in the Supporting Information. During the experiment, we found that at least 1 h is needed for the NW to recover to its original state in the dark. For this reason, the photogating effect will last for a very long period of time, so that these InAs NW transistors can not only be used in sensitive photodetectors, but also in light-induced current amplifiers under negative back-gate voltage modulation. Figure S6 in the Supporting Information gives the photoresponse of other three InAs NW transistors under a gate voltage of –40 V. It can be seen from Figure S6a in the Supporting Information that the enhancement of I_{off} can be maintained for a long time. In addition, the increments of the currents (ΔI) among these devices are different, wherein the difference originates from the different trapping capacities of PGLs between NWs. The more holes in the PGL are trapped, the higher the positive photogate (ΔV_{gh}) that is formed in the PGL, which induces an increase of the current. In fact, ΔV_{gh} can also offset a fraction of the negative ΔV_{ge} during the light-exposure process (see Figure S5b,e in the Supporting Information). In our experiment, the negative photogate is dominant due to the accumulation of more photoexcited electrons in the PGL than holes, and the effect of depletion in the channel is still strong. This is the reason why I_{on} can maintain a stable low current with time under different gate voltages.

To investigate the sensitivity of the phototransistor, we performed photoresponse measurements under different light intensities, and results are shown in **Figure 4**a, from which $I_{off}/I_{on} \approx 133$, 125, and 30 can be obtained under light intensities of 8, 4, and 0.8 mW mm^{-2}, respectively, at $V_{gs} = 0$ V and $V_{ds} = 1$ V; I_{off} and I_{on} decreases and increases with the decay of light power, accordingly. This is because, at the low intensity of incident light, fewer electron–hole pairs are generated, so that more electrons remain in the core during the recombination and depletion process to contribute to I_{on}. Simultaneously, no additional holes trapped in the PGL leads to a weakened ΔV_{gh}, and hence the negative ΔV_{ge} is dominant and reduces I_{off}. As shown in Figure 4b, the relation between I_{off} and light intensity obeys the power law[13,15,20,42] $I = cP^k$, where P is the light intensity, c is a proportionality constant, and k is an empirical value. By fitting the measured data with the equation, we obtain $c = 1$ and $k = 0.35$. This relation further demonstrates that the current of I_{off} is indeed from the contribution of accumulated photoexcited electrons in the PGL. The non-integer power

 © 2014 WILEY-VCH Verlag GmbH & Co. KGaA, Weinheim

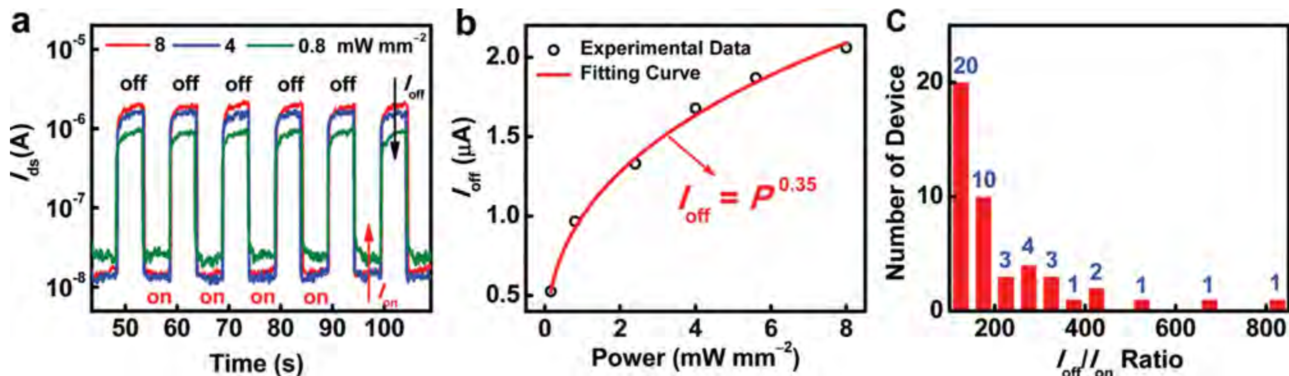

Figure 4. Power dependence of photoresponse. a) Photoresponse properties of the InAs NW transistor under green laser illumination (532 nm) at $V_{gs} = 0$ V and $V_{ds} = 1$ V in air, acquired for different light intensities: 0.8, 4 and 8 mW mm^{-2}. The photoconductance modulation is induced by manipulating a shutter for the light on/off at an interval of 5 s. b) I_{off} versus light intensity, from the data shown in Figure 4a and Figure S7 in the Supporting Information. c) Histogram of I_{off}/I_{on} ratio of all 46 fabricated InAs NW transistors, acquired under illumination from a green laser (532 nm, 8 mW mm^{-2}) at $V_{gs} = 0$ V and $V_{ds} = 1$ V in air.

law ($k < 1$) suggests a complex carrier-transfer process, as discussed in Figure S5a–c in the Supporting Information. The photoresponse measured under the other three light intensities is presented in Figure S7 in the Supporting Information. In this study, we examined 46 InAs NW transistors with channel lengths between 2.0 and 3.5 μm, and statistics results of the I_{off}/I_{on} ratio are shown in Figure 4c. As can be seen, all of these 46 devices exhibit an ultrahigh negative photoresponse. Four typical samples from these 46 devices are shown in Figure S8 in the Supporting Information.

After the above discussion, it can be found that the photocurrents no longer rely on the junction region. In order to testify this point, we intentionally found a long InAs NW fabricated into a multielectrode transistor to study the position dependence of the photoelectric characteristics. As shown in **Figure 5**a, the NW is contacted with 3 metallic electrodes, each of them 2 μm wide, and separated into two parts. Three channels, i.e., CH1, CH2, and CH3, are formed along the NW with channel lengths of 3, 1.5, and 6.5 μm, respectively. Figure 5b gives I_{ds}–V_{ds} characteristics of the as-fabricated InAs NW transistor in the dark and under illumination by a green laser (532 nm, 8 mW mm^{-2}) in air. The relation of the photocurrents between these three channels is $I_{Light\text{-}CH1} > I_{Light\text{-}CH2} \approx I_{Light\text{-}CH3}$. The photocurrent of CH3 totally depends on that of CH2. It is easy to understand that the resistance of CH3 depends on the portion that has the greatest resistance along the NW under light excitation, i.e., CH2 in this case. Therefore, a high performance of a photodetector can be easily obtained as long as one small part of the NW is sensitive.

The performance of the InAs NW transistor under near-infrared light illumination at room temperature has been studied. Figure 5c gives the I_{ds}–V_{ds} properties acquired under light illumination at a wavelength of 1.2 μm (another sample in our work). It can be seen that the photocurrents decrease significantly due to the mechanism discussed above. A photoconductive gain of −1.1 is obtained at $V_{ds} = 2$ V and repeated measurements prove that the device has a good stability. In addition, it is obvious that the device performs with a higher negative response to visible light than that to near-infrared light, in comparison with the data in Figure 5b. This may be because

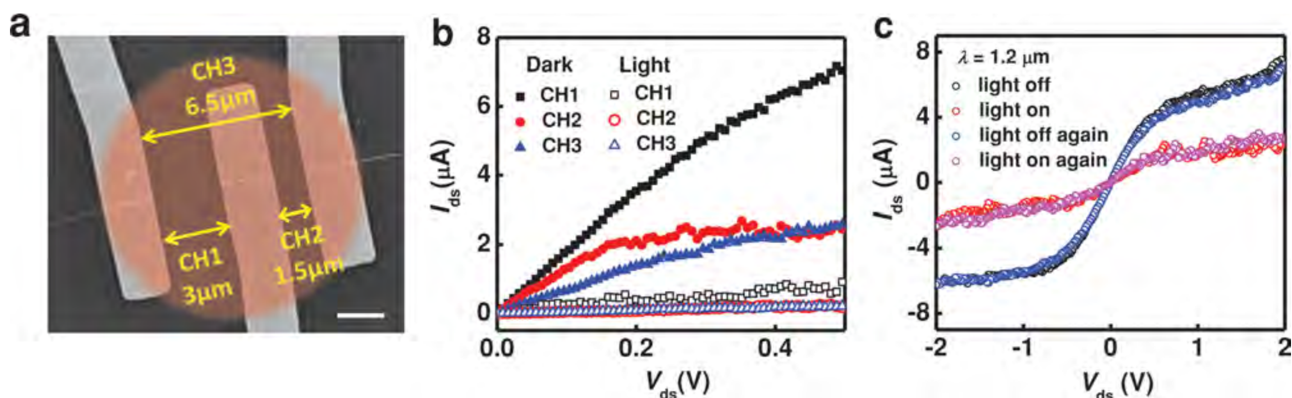

Figure 5. Position dependence of photoresponse and near-infrared measurement. a) SEM image of the InAs NW transistor. The NW is contacted with 3 metallic electrodes, each of them 2 μm wide, and separated into two parts. Three channels along the NW are formed, i.e., CH1, CH2, and CH3 with channel lengths of 3, 1.5, and 6.5 μm, respectively. The scale bar is 2 μm. b) I_{ds}–V_{ds} curves of the multielectrode InAs NW transistor in the dark (closed symbols) and under illumination from a green laser (532 nm, 8 mW mm^{-2}) (open symbols) at V_{gs} of 0 V in air, recorded for different conductive channels CH1, CH2, and CH3. c) I_{ds}–V_{ds} curves of the InAs NW transistor under near-infrared light excitation at $V_{gs} = 0$ V in air.

© 2014 WILEY-VCH Verlag GmbH & Co. KGaA, Weinheim

high-energy photons excite the photocarriers into the PGL more efficiently, leading to a stronger negative photogate to modulate the channel conductance.

In summary, we have demonstrated InAs NW phototransistors based on the majority-carrier-dominated photodetection mechanism. A high photoconductive gain of approximately $\approx 10^5$ and a fast response time of 12 ms are obtained at room temperature. Further analysis shows that the high device performance originates from the trapping mechanism of the self-assembled, near-surface PGL, which leads to a strong photogating effect on the NW channel by capturing photocarriers. Moreover, the photodetection, which is free from environmental impact, makes the device more widely applicable. Majority carriers contributing the photocurrents, this new phenomenon and related properties will pave a way to enable novel high-sensitivity broad-spectrum room-temperature detection.

Experimental Section

Nanowire Growth: InAs NWs used in this study were prepared by a solid-source CVD method. In brief, InAs powders (1.2 g; 99.9999% purity) were heated in the upstream source zone of a two-zone tube furnace and the evaporated precursors were transported by a carrier gas of H_2 (99.999% purity; 200 sccm) to the downstream substrate zone. For this two-step growth scheme, a 0.5 nm thick Ni catalyst film pre-deposited on SiO_2/Si substrates was employed and annealed at 800 °C for 10 min. The pressure was maintained at ca. 3.0 Torr for the entire process. After that, the substrate temperature was first lowered to the nucleation temperature of 560 °C in the downstream zone. When the source temperature reached the designated value of 690 °C in the upstream zone, the nucleation of NWs began. After 2 min, the downstream temperature was further lowered to the second step-growth temperature of 470 °C and maintained for 20 min. Finally, the substrates were cooled to room temperature naturally.

There are two most likely factors in our case for the reason for the formation of the defected shell. One is that the source temperature (upstream zone) is relatively high 690 °C, providing more than enough source vapors to create catalytic supersaturation for the NW growth, and the excess source vapor will react non-uniformly on the NW surface to induce the defects. The other is that the process pressure, ca. 3.0 Torr, is too high, inducing a shorter mean-free path of the precursor vapor, and thus forming the defects.

Phototransistor Fabrication and Characterization: The InAs NWs were transferred mechanically to pre-cleaned p^+-Si/SiO_2 (300 nm) substrates. Then, electron-beam lithography (JEOL 6510 with an NPGS System) was used to define the S/D patterns. Before metallization, the NWs were dipped into a 2%HF solution for ca. 10 s to remove the native oxide to ensure the formation of Ohmic contact between the metal electrode (15 nm Cr/60 nm Au) and the NW. The optoelectronic properties of the fabricated devices were characterized using a Lake Shore TTPX Probe Station together with an Agilent 4155C semiconductor parameter analyzer.

Supporting Information

Supporting Information is available from the Wiley Online Library or from the author.

Acknowledgements

The authors acknowledge J. Torley for critical reading of the manuscript. This work was supported in part by the 973 grant of MOST (Nos. 2014CB921600 and 2013CB632705), the NSFC (grant nos. 11322441, 11274331, 11334008, 61376015, and 11104207), the Shanghai Rising-Star Program, Fund of Shanghai Science and Technology Foundation (14JC1406400), the Early Career Scheme of the Research Grants Council of Hong Kong SAR, China (CityU 139413), and the Australian Research Council. The authors thank X. Bai, T. Li, P. Chen and X. Tian for technical assistance.

Received: August 10, 2014
Revised: September 18, 2014
Published online: October 28, 2014

[1] K. Takei, T. Takahashi, J. C. Ho, H. Ko, A. G. Gillies, P. W. Leu, R. S. Fearing, A. Javey, *Nat. Mater.* **2010**, *9*, 821.
[2] D. Saxena, S. Mokkapati, P. Parkinson, N. Jiang, Q. Gao, H. H. Tan, C. Jagadish, *Nat. Photonics* **2013**, *7*, 963.
[3] M. S. Gudiksen, L. J. Lauhon, J. F. Wang, D. C. Smith, C. M. Lieber, *Nature* **2002**, *415*, 617.
[4] Y. Huang, X. F. Duan, Y. Cui, L. J. Lauhon, K. H. Kim, C. M. Lieber, *Science* **2001**, *294*, 1313.
[5] J. Wallentin, N. Anttu, D. Asoli, M. Huffman, I. Åberg, M. H. Magnusson, G. Siefer, P. Fuss-Kailuweit, F. Dimroth, B. Witzigmann, H. Q. Xu, L. Samuelson, K. Deppert, M. T. Borgström, *Science* **2013**, *339*, 1057.
[6] J. Y. Tang, Z. Y. Huo, S. Brittman, H. W. Gao, P. D. Yang, *Nat. Nanotechnol.* **2011**, *6*, 568.
[7] S. Ju, A. Facchetti, Y. Xuan, J. Liu, F. Ishikawa, P. D. Ye, C. W. Zhou, T. J. Marks, D. B. Janes, *Nat. Nanotechnol.* **2007**, *2*, 378.
[8] D. C. Dillen, K. Kim, E. S. Liu, E. Tutuc, *Nat. Nanotechnol.* **2014**, *9*, 116.
[9] T. Takahashi, K. Takei, E. Adabi, Z. Y. Fan, A. M. Niknejad, A. Javey, *ACS Nano* **2010**, *4*, 5855.
[10] A. C. Ford, J. C. Ho, Y. L. Chueh, Y. C. Tseng, Z. Y. Fan, J. Guo, J. Bokor, A. Javey, *Nano Lett.* **2009**, *9*, 360.
[11] N. Han, F. Y. Wang, J. J. Hou, S. P. Yip, H. Lin, F. Xiu, M. Fang, Z. X. Yang, X. L. Shi, G. F. Dong, T. F. Hung, J. C. Ho, *Adv. Mater.* **2013**, *25*, 4445.
[12] S. A. Dayeh, D. P. R. Aplin, X. T. Zhou, P. K. L. Yu, E. T. Yu, D. L. Wang, *Small* **2007**, *3*, 326.
[13] H. Kind, H. Q. Yan, B. Messer, M. Law, P. D. Yang, *Adv. Mater.* **2002**, *14*, 158.
[14] J. J. Wang, F. F. Cao, L. Jiang, Y. G. Guo, W. P. Hu, L. J. Wan, *J. Am. Chem. Soc.* **2009**, *131*, 15602.
[15] S. C. Kung, W. E. Van der Veer, F. Yang, K. C. Donavan, R. M. Penner, *Nano Lett.* **2010**, *10*, 1481.
[16] Y. H. Ahn, J. Park, *Appl. Phys. Lett.* **2007**, *91*, 162102.
[17] Z. Wang, M. Safdar, C. Jiang, J. He, *Nano Lett.* **2012**, *12*, 4715.
[18] G. Chen, B. Liang, X. Liu, Z. Liu, G. Yu, X. M. Xie, T. Luo, D. Chen, M. Q. Zhu, G. Z. Shen, Z. Y. Fan, *ACS Nano* **2014**, *8*, 787.
[19] Z. Liu, G. Chen, B. Liang, G. Yu, H. T. Huang, D. Chen, G. Z. Shen, *Opt. Express* **2013**, *21*, 7799.
[20] P. C. Wu, Y. Dai, Y. Ye, Y. Yin, L. Dai, *J. Mater. Chem.* **2011**, *21*, 2563.
[21] C. Soci, A. Zhang, B. Xiang, S. A. Dayeh, D. P. R. Aplin, J. Park, X. Y. Bao, Y. H. Lo, D. Wang, *Nano Lett.* **2007**, *7*, 1003.
[22] J. S. Miao, W. D. Hu, N. Guo, Z. Y. Lu, X. Y. Zou, L. Liao, S. X. Shi, P. P. Chen, Z. Y. Fan, J. C. Ho, T. X. Li, X. S. Chen, W. Lu, *ACS Nano* **2014**, *8*, 3628.
[23] P. C. Wu, Y. Dai, T. Sun, Y. Ye, H. Meng, X. L. Fang, B. Yu, L. Dai, *ACS Appl. Mater. Interfaces* **2011**, *3*, 1859.
[24] Q. Hang, F. Wang, P. D. Carpenter, D. Zemlyanov, D. Zakharov, E. A. Stach, W. E. Buhro, D. B. Janes, *Nano Lett.* **2008**, *8*, 49.
[25] Y. H. Ahn, J. Dunning, J. Park, *Nano Lett.* **2005**, *5*, 1367.

© 2014 WILEY-VCH Verlag GmbH & Co. KGaA, Weinheim

[26] S. Thunich, L. Prechtel, D. Spirkoska, G. Abstreiter, A. F. Morral, A. W. Holleitner, *Appl. Phys. Lett.* **2009**, *95*, 083111.
[27] J. Zhou, Y. Gu, Y. Hu, W. Mai, P. H. Yeh, G. Bao, A. K. Sood, D. L. Polla, Z. L. Wang, *Appl. Phys. Lett.* **2009**, *94*, 191103.
[28] C. H. Lin, T. T. Chen, Y. F. Chen, *Opt. Express* **2008**, *16*, 16916.
[29] M. W. Chen, C. Y. Chen, D. H. Lien, Y. Ding, J. H. He, *Opt. Express* **2010**, *18*, 14836.
[30] T. J. Kempa, B. Z. Tian, D. R. Kim, J. S. Hu, X. L. Zheng, C. M. Lieber, *Nano Lett.* **2008**, *8*, 3456.
[31] M. Heurlin, P. Wickert, S. Fält, M. T. Borgström, K. Deppert, L. Samuelson, M. H. Magnusson, *Nano Lett.* **2011**, *11*, 2028.
[32] Y. Guo, Y. Zhang, H. Liu, S. W. Lai, Y. Li, Y. Li, W. Hu, S. Wang, C. M. Che, D. Zhu, *J. Phys. Chem. Lett.* **2010**, *1*, 327.
[33] W. Wei, X. Y. Bao, C. Soci, Y. Ding, Z. L. Wang, D. Wang, *Nano Lett.* **2009**, *9*, 2926.
[34] S. P. Mondal, S. K. Ray, *Appl. Phys. Lett.* **2009**, *94*, 223119.
[35] Z. Guo, D. X. Zhao, Y. C. Liu, D. Z. Shen, J. Y. Zhang, B. H. Li, *Appl. Phys. Lett.* **2008**, *93*, 163501.
[36] H. Zhou, G. Fang, L. Yuan, C. Wang, X. Yang, H. Huang, C. Zhou, X. Zhao, *Appl. Phys. Lett.* **2009**, *94*, 013503.
[37] G. Konstantatos, M. Badioli, L. Gaudreau, J. Osmond, M. Bernechea, F. P. G. Arquer, F. Gatti, F. H. L. Koppens, *Nat. Nanotechnol.* **2012**, *7*, 363.
[38] C. H. Liu, Y. C. Chang, T. B. Norris, Z. H. Zhong, *Nat. Nanotechnol.* **2014**, *9*, 273.
[39] H. J. Joyce, Q. Gao, H. H. Tan, C. Jagadish, Y. Kim, X. Zhang, Y. Guo, J. Zou, *Nano Lett.* **2007**, *7*, 921.
[40] J. J. Hou, N. Han, F. Wang, F. Xiu, S. P. Yip, A. T. Hui, T. Hung, J. C. Ho, *ACS Nano* **2012**, *6*, 3624.
[41] W. Choi, M. Y. Cho, A. Konar, J. H. Lee, G. B. Cha, S. C. Hong, S. Kim, J. Kim, D. Jena, J. Joo, S. Kim, *Adv. Mater.* **2012**, *24*, 5832.
[42] Y. Jiang, W. J. Zhang, J. S. Jie, X. M. Meng, X. Fan, S. T. Lee, *Adv. Funct. Mater.* **2007**, *17*, 1795.

© 2014 WILEY-VCH Verlag GmbH & Co. KGaA, Weinheim